ChemComm

Live-Cell Imaging of Multiple Endogenous mRNAs Permits Direct Observation of RNA Granule Dynamics

Journal:	*ChemComm*
Manuscript ID	CC-COM-05-2018-003805.R1
Article Type:	Communication

Journal Name

COMMUNICATION

Live-Cell Imaging of Multiple Endogenous mRNAs Permits Direct Observation of RNA Granule Dynamics

Received 00th January 20xx,
Accepted 00th January 20xx

DOI: 10.1039/x0xx00000x

www.rsc.org/

Kenji Yatsuzuka,[a] Shin-ichi Sato,*[a] Kathleen Beverly Pe,[a] Yousuke Katsuda,‡[a] Ippei Takashima,[a] Mizuki Watanabe §[a] and Motonari Uesugi *[ab]

Here, we developed two pairs of high-contrast chemical probes and their RNA aptamers with distinct readout channels that permitted simultaneous live-cell imaging of endogenous β-actin and cortactin mRNAs. Application of the technology allowed direct observation of the formation process of stress granules, protein-RNA assemblies essential for cellular response to environment.

The spatiotemporal dynamics of mRNA plays important roles in protein expression. Non-translating mRNAs usually form non-membrane-bound organelles, so-called RNA granules, which are classified into two classes: (i) processing bodies (P-bodies) that regulate mRNA turnover; and (ii) stress granules, whose formation is accelerated upon cellular stress.[1] In mammalian cells, P-bodies and stress granules dock and undock from one another[2], suggesting that mRNAs inside these two granules are exchanged between them. Analysis of how the RNA-containing granules interact, and how endogenous mRNAs inside them are exchanged, is important for understanding how cells traffic-control cytosolic mRNAs. Live-cell imaging of mRNAs inside granules would be useful for this purpose. Although an increasing number of methods for live-cell RNA imaging have been developed, including the MS2[3] and Spinach[4] systems, these seminal methods permit detection of only tagged or engineered mRNA. A few methods have been reported for the live-cell detection of native, non-engineered mRNA, including the pioneering methods represented by molecular beacon and related oligonucleotide probes.[5] The high designability for specific RNA targets permits visualization of a wide range of endogenous RNAs. However, several challenges remain. For example, low stability of the beacons in cells produces relatively high background fluorescence. Another recently developed approach uses hybrid proteins that combine split GFP and RNA-binding proteins.[6] This genetically encoded approach has provided valuable information about the dynamics of endogenous RNAs. The primary drawback of this method is the need to design a specific probe for each RNA target.

We and others previously described a live-cell RNA imaging method that potentially overcomes these limitations.[7] The method combines a tailor-made RNA aptamer with a cell-permeable, quenched fluorescent chemical probe. In our method[7b], the chemical probe is conjugated with BHQ1, a black hole quencher, and its quenched fluorescence is restored when the BHQ1 segment binds to the RNA aptamer in the presence of the mRNA of interest. When the RNA aptamer, which is encoded by a transfected plasmid, hybridizes to a complementary sequence in the target mRNA, it forms a binding loop for BHQ1 to restore the fluorescence of the conjugate. This versatile method permits visualization of non-engineered, endogenous mRNAs in living cells. Development of simple approaches to simultaneously imaging of multiple RNAs is essential to gain deeper insights into the functions and dynamics of RNA in cells. In the present study, we aimed to complement and advance our previous work by designing optimized, high-contrast chemical probes with distinct readout channels that permitted simultaneous live-cell imaging of RNA granule dynamics and interactions (**Figure 1**).

We previously showed that the quenched BHQ1-sulfoCy3 conjugate probe (**1**, **Figure 1A**) became fluorogenic upon binding to a BHQ1-binding aptamer. However, it remained unclear exactly how binding to the aptamer turned on the fluorescence. Quenching of such turn-on probes is often mediated by intermolecular or intramolecular contacts, and BHQ1 is also a fluorescence resonance energy transfer (FRET) type quencher. Therefore, we reasoned that the quenching of BHQ1-sulfoCy3 conjugate probe (**1**) is mediated by a combination of contact quenching and FRET mechanisms.

To examine the contribution of contact quenching, we measured the UV spectra of BHQ1-sulfoCy3 conjugate probe

[a] *Institute for Chemical Research, Kyoto University, Uji, Kyoto 611-0011, Japan. E-mail: ssato@scl.kyoto-u.ac.jp, uesugi@scl.kyoto-u.ac.jp*
[b] *Institute for Integrated Cell-Material Sciences (WPI-iCeMS), Kyoto Universit y, Uji, Kyoto 611-0011, Japan. E-mail: uesugi@scl.kyoto-u.ac.jp*
†Electronic Supplementary Information (ESI) available: [details of any supplementary information available should be included here]. See DOI: 10.1039/x0xx00000x
‡Present address: Division of Materials Science, Faculty of Advanced Science and Technology, Kumamoto University, Kumamoto 860-8555, Japan.
§Present address: Faculty of Pharmaceutical Sciences, Hokkaido University, Kita-12, Nishi-6, Kita-ku, Sapporo 060-0812, Japan.

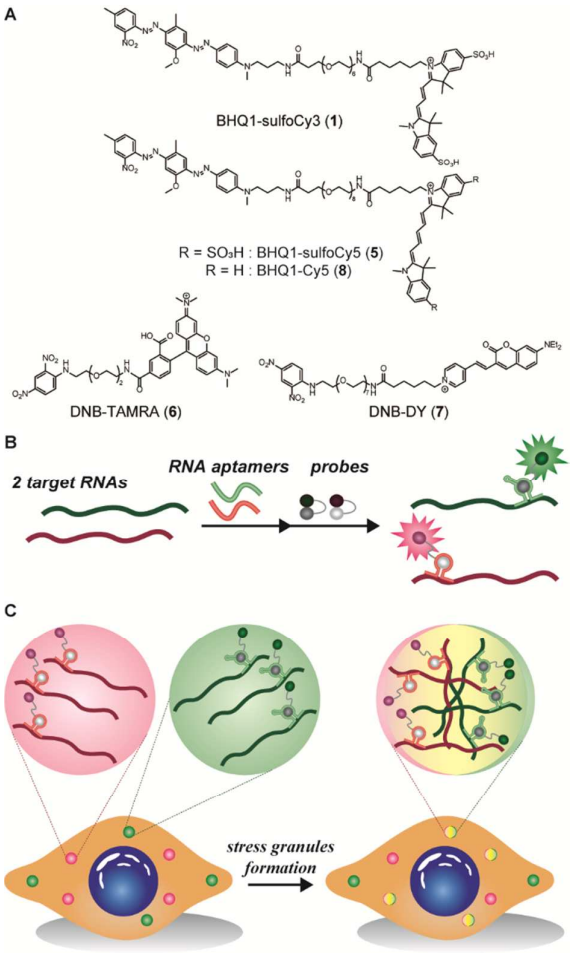

Fig. 1 Schematic representation of the RNA imaging method described in this study. (A) Chemical structures of the probes used in this work. (B) Each RNA aptamer hybridizes with its target RNA to form a quencher-binding loop. Interaction of the loop with its corresponding probe restores fluorescence of the probe. (C) Multicolor RNA imaging in living cells. Introduction of aptamer expression vectors and probes into identical cells allows simultaneous detection of subsets of mRNA granules. The multicolor imaging method permits direct observation of the formation of stress granules in response to cellular stress.

(**1**), sulfoCy3, and BHQ1 in an aqueous buffer (**Figure S1B**). Probe **1** exhibited a UV spectrum distinct from the combined spectrum of sulfoCy3 and BHQ1, suggesting that the ground electronic states of sulfoCy3 and BHQ1 in the conjugate are different from those of the molecules standing alone. In contrast, addition of a BHQ1-binding aptamer (A1) rendered the UV spectrum of the conjugate analogous to the combined spectra of sulfoCy3 and BHQ1 (**Figure S1C**). These results suggest that the interaction of the aptamer with the BHQ1 segment of probe **1** releases its physical contacts with sulfoCy3, making sulfoCy3 more susceptible to photo excitation.[8] Two-dimensional NOESY spectra of probe **1** revealed a number of NOE signals between sulfoCy3 and BHQ1 in 50% (v/v) D_2O/DMSO-d_6, but not in 100% DMSO-d_6, supporting the notion that these two groups of probe **1** are in close proximity in an aqueous solution (**Figure S2**).

In addition to the contact inhibition mechanism, FRET is thought to play a role in quenching the fluorescence of probe conjugate **1**. A remaining question is whether BHQ1 maintains its ability to exert FRET for quenching when in complex with the aptamer. The UV absorbance profile of BHQ1 exhibited no detectable alteration, even in the presence of the BHQ1-binding aptamer, suggesting that aptamer-bound BHQ1 is likely to maintain its property for exerting FRET (**Figure S3**). In fact, the fluorescence intensity of the aptamer-bound probe is 70 times lower than that of sulfoCy3 (**Figure S4**).

One approach to improving the signal-to-background ratio of probe **1** is to optimize its fluorescence intensity upon binding to the aptamer. As the efficiency of FRET is inversely proportional to the sixth power of the distance between the donor and acceptor, introduction of a longer linker to probe **1** would reduce the effect of the residual FRET after the BHQ1-binding aptamer releases the physical contacts between BHQ1 and sulfoCy3. We synthesized two BHQ1-sulfoCy3 conjugates with longer linkers (probes **2** and **3**) and analysed their ability to restore fluorescence upon binding to the aptamer. Lengthening the poly(ethylene glycol) linker significantly increased fluorescence intensity upon binding to the BHQ1-binding aptamer. Conversely, probe **4** with a shorter linker displayed lower fluorescence intensity than the parental probe (**1**) (**Table S1**, **Figure S5**). We selected probe **2** for further optimization.

Another approach to improving the signal-to-background ratio is to reduce the background signal of unbound probe **2**. Physicochemical properties of fluorophores usually govern the extent of contact-induced fluorescence quenching effects. Therefore, we replaced sulfoCy3 of probe **2** with six different fluorophores (**Table S2**). The probe with sulfoCy5 (probe **5**, **Figure 1A**) showed the lowest background, with a signal-to-background ratio of 20 (**Figure S6**). We used probe **5** for subsequent multicolor imaging.

To achieve multicolor imaging, we needed to pair a chemical probe equipped with a distinct quencher and its partner RNA aptamer. As a new quencher, we selected 1,3-dinitrobenzen (DNB), a low molecular weight, low hydrophobic quencher that has been used in a number of imaging studies[7d, 9]. To obtain an RNA aptamer for DNB, we carried out *in vitro* selection of an RNA library comprising 60-base random sequences (**Figure S7**, **Table S4**). Eight rounds of selection yielded four DNB-binding RNA aptamers with sequences conserved in all four (DNB1-4), and another conserved in only three (DNB1-3) (**Figure S8A**). Their ability to bind to DNB was evaluated using a DNB-TAMRA probe (**6**, **Figure 1A**). Fluorescence measurement revealed that DNB1-3 restored the fluorescence of the probe, while DNB4 failed to do so (**Figure S8B, C**), indicating that both of the conserved sequences are required for the interaction. We selected the most sensitive DNB1 for further analysis.

Secondary structure prediction of DNB1, calculated by CentroidFold (http://rtools.cbrc.jp/centroidfold/), suggested a stem-loop structure in which the two conserved sequences form an internal loop (**Figure 2A**). To validate the model, we designed a simplified aptamer (DNB1-short), in which minimal essential RNA segments for the formation of the internal loop were maintained (**Figure 2B**). Indeed, DNB1-short restored the

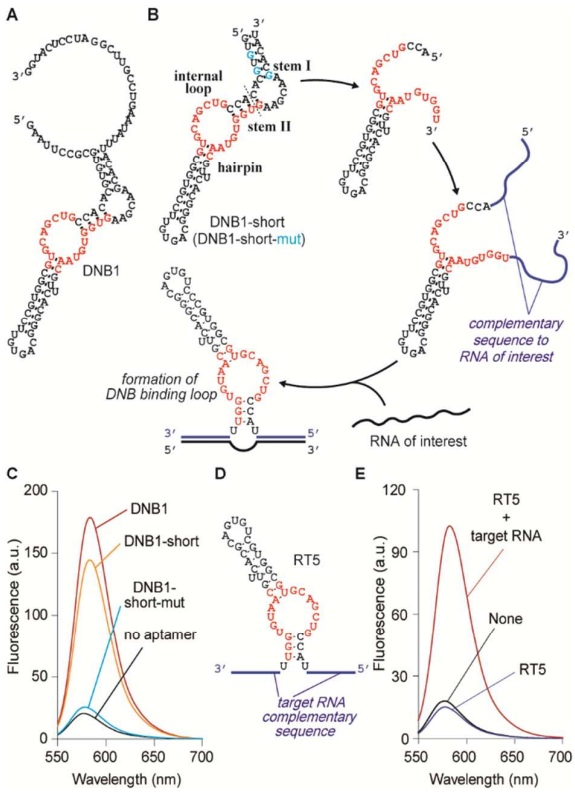

Fig. 2 DNB aptamers. (A) Predicted secondary structure of DNB1 aptamer. (B) Design of DNB1-short and DNB1-short-mut aptamers and outline of the design. Truncation of the stem regions and introduction of sequences complementary to that of the target RNA regenerate the DNB-binding stem-loop structure only in the presence of the target RNA. Three G bases marked by blue color were converted to C bases in DNB1-short-mut. (C) Fluorescence emission spectra of probe 6 in the presence of DNB1, DNB1-short, or DNB1-short-mut aptamers. (D) Sequence and potential secondary structure of RT5 aptamer. (E) Fluorescence emission spectra of probe 6 with RT5 aptamer in the absence (blue) and presence (red) of the target RNA.

fluorescence of the probe to the same level as DNB1 (**Figure 2C**). We further designed a point mutant of DNB1-short (DNB1-short-mut), in which three guanines were replaced by three cytosines (**Figure 2B**). This replacement would unfold the internal loop by disassembling or destabilizing stem I and II structures. As expected, DNB1-short-mut failed to restore the fluorescence of the probe (**Figure 2C**). These results collectively provide support for the predicted secondary structure.

Taking advantage of the stem-loop structure of DNB1-short, we next aimed to design a DNB aptamer that is responsive to an RNA of interest. Cleavage of stem II in DNB1-short would disassemble the DNB-binding stem-loop structure and thereby impair its ability to bind to DNB. We envisioned that introducing sequences complementary to that of the target RNA to the ends of the cleaved aptamer would regenerate the DNB-binding stem-loop structure only in the presence of the target RNA (**Figure 2B**). Such consideration led to the design of an aptamer that was equipped with a 16-base complementary sequence at each end (RT1). As expected, the designed aptamer restored the fluorescence of the probe in the presence of the 36-base target RNA (**Figure S9**). However, we detected a slight increase of fluorescence even in the absence of the target RNA, suggesting the existence of persistent target RNA-independent affinity of RT1 to DNB. To further destabilize the DNB-binding stem-loop structure, we designed three additional aptamers with shorter stem II sequences (RT2-4). RT2, with a one-bp shorter stem II, exhibited an improved signal-to-background ratio, due to reduced background fluorescence in the absence of the target RNA. Further shortening in RT3 and 4 impaired the ability of the aptamers to restore the fluorescence of the probe, possibly due to their inability to fold into the DNB-binding stem-loop structure in the presence of the target RNA.

We selected RT2 for further simplification, and designed truncated versions, RT5-7, in which the upper hairpin structure was shortened. RT5 showed similar ability to RT2 in restoring the fluorescence of the probe, while RT6 and 7 exhibited lower signal-to-background ratios than RT2. RT5 was selected for subsequent live-cell imaging studies (**Figure 2D, E**).

To further improve the signal-to-background ratio, we optimized the DNB-TAMRA probe (**6**) by replacing TAMRA with each one of six different fluorophores, just as we did for the BHQ1-sulfoCy3 probe (**1**). Fluorescence of these DNB conjugate probes were monitored in the absence or presence of DNB1, a DNB-binding aptamer. The DNB probe conjugated with 1-(5-carboxy-pentyl)-4-[(*E*)-2-(7-diethylamino-2-oxo-2*H*-chromen-3-yl)-vinyl]-pyridinium (DNB-DY, probe **7**) displayed an excellent signal-to-background ratio of 156 (**Figure S10**), and showed no detectable cross-responses to the BHQ1-binding aptamer A1. Furthermore, the DNB1 aptamer had no detectable effect on fluorescence of BHQ1 conjugate probe **5** (**Figure S11**). These results suggest that these two high-contrast probes and their corresponding aptamers can be exploited for simultaneous imaging of multiple mRNAs in cells.

For proof of concept, we first attempted multicolor imaging of β-actin mRNA in fixed HeLa cells. We designed DNB-binding (RT5) and BHQ1-binding aptamers that recognize distinct sequences within β-actin mRNA. Upon binding to β-actin mRNA, the custom-designed aptamers should form loop structures required for their association with DNB and BHQ1, colocalizing fluorescence signals from DNB-conjugate probe **7** and BHQ1-conjugate probe **5** (**Figure S12Aa**). Indeed, confocal microscopic observation revealed that both probes **5** and **7** permitted detection of β-actin mRNA-containing RNA granules. Dot-like morphologies of the RNA granules are consistent with those observed in our previous report[7b]. As expected, probe **7**-derived green signals overlapped with probe **5**-derived red signals (Pearson's R: 0.64) (**Figure S12Ba**).

We have carried out similar experiments with mRNA of cortactin, an actin-related cytoskeletal protein (**Figure S12Ad**), and found overlapping images of signals from probes **5** and **7** (Pearson's R: 0.77) (**Figure S12Bd**). In contrast, when each aptamer was designed to recognize a different mRNA (**Figure S12Ab**,**c**), each probe detected a distinct set of RNA granules (Pearson's R: 0.18 and 0.14), suggesting that mRNAs of β-actin and cortactin accumulate in different RNA granules (**Figure S12Bb**,**c**). This observation is consistent with previous FISH results[10].

Encouraged by the results in fixed cells, we proceeded to multicolor imaging of β-actin and cortactin mRNAs in living cells. The same aptamers used in fixed cell experiments were coexpressed in living HeLa cells through transfection of short-RNA expression vectors encoding the aptamers. Probe **7** was similarly used for live-cell imaging, while probe **5** was replaced by its cell-permeable version (probe **8**)[7b]. When identical mRNA was targeted, fluorescence signals were colocalized (Pearson's R: 0.83); when different mRNAs was targeted, signals exhibited little colocalization (Pearson's R: 0.11) (**Figure S13**, **Movie S1–5**). However, distributions of the fluorescence signals in live cells were somewhat different from those in fixed cells. The fixation procedure might have possibly affected the localization of RNA granules. Overall, these results demonstrate that our method permits simultaneous detection of multiple endogenous, non-engineered mRNAs in living cells.

We next attempted to observe the dynamics of β-actin and cortactin mRNAs during stress-granule formation in living HeLa cells. Stress granules are dense aggregations that absorb surrounding free RNAs and RNA granules in response to various types of stress, such as arsenite, heat shock, hypoxia, and viral infections[1]. Upon exposure to arsenite (500 μM), mRNA granules containing β-actin and cortactin mRNAs (red and green dots, respectively) started colocalizing to form slightly larger granules (**Figure 3, Movie S6–8**). Time-lapse live-cell imaging showed that the fusion of the RNA granules was initiated immediately after addition of arsenite, and was completed within 14 minutes when the majority of fluorescence signals came together in the cytosol (Pearson's R: 0.81).

Stress granules have been hypothesized to protect cells from cellular stress via translational repression and RNA storage. Previous analysis suggested that stress granules are fused products of RNA granules and that their components are dynamically exchanged among other granules[2]. Interestingly, a subset of the molecules within stress granule components exchange more slowly than others. Perhaps the components in the core layer of stress granules are less dynamic than those in the shell structure[11]. Despite the knowledge gained by these previous studies, the dynamic process of stress granule formation has been unclear. Our multicolor live-cell method, detecting internal mRNA components, sheds a light on direct live-cell observation of stress granule formation.

Two limitations remain in our RNA-imaging technology: (i) detection is highly dependent on the local concentration of a target endogenous mRNA, and (ii) target sequences in the mRNA of interest must be carefully selected. These limitations could potentially be solved by (i) further optimization of probes and (ii) targeting sequences known for effective siRNA silencing. Further improvement of the RNA-imaging method described here may prove useful for studying stress granules and other RNA-containing organelles.

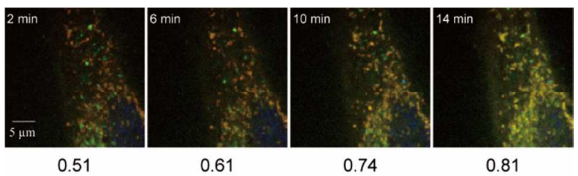

Fig. 3 Live-cell time-lapse image of β-actin mRNA (red dots) and cortactin mRNA (green dots) under cellular stress induced by adding $NaAsO_2$ (500 μM). Staining of the nuclei with Hoechst 33342 is shown in blue. Co-localisation between β-actin mRNA and cortactin mRNA was quantified by ImageJ. Pearson's correlation coefficient values (Pearson's R) are shown at the bottom.

This work is supported in part by JSPS (26220206 to M.U. and 17K19200 to S.S.), JST (AS242Z01268P to S.S.), FY2017 Kyoto University Research Development Program, ISHIZUE (to S.S.) and ZE Research Program, IAE (ZE29B17 to S.S.). 600-MHz NMR analyses and FT-ICR-MS analyses were supported by JURC at ICR, KU, Japan.

Conflicts of interest

There are no conflicts to declare.

Notes and references

1 (a) J. R. Buchan, *RNA Biol.*, 2014, **11**, 1019-1030; (b) P. Anderson and N. Kedersha, *Nat. Rev. Mol. Cell Biol.*, 2009, **10**, 430-436; (c) R. Parker and U. Sheth, *Mol. Cell*, 2007, **25**, 635-646; (d) A. Eulalio, I. Behm-Ansmant and E. Izaurralde, *Nat. Rev. Mol. Cell Biol.*, 2007, **8**, 9-22.

2 (a) J. R. Buchan, D. Muhlrad and R. Parker, *J. Cell Biol.*, 2008, **183**, 441-455; (b) N. Kedersha, G. Stoecklin, M. Ayodele, P. Yacono, J. Lykke-Andersen, M. J. Fritzler, D. Scheuner, R. J. Kaufman, D. E. Golan and P. Anderson, *J. Cell Biol.*, 2005, **169**, 871-884.

3 (a) E. Bertrand, P. Chartrand, M. Schaefer, S. M. Shenoy, R. H. Singer and R. M. Long, *Mol. Cell*, 1998, **2**, 437-445; (b) S. Mili, K. Moissoglu and I. G. Macara, *Nature*, 2008, **453**, 115-119; (c) Y. Shav-Tal, X. Darzacq, S. M. Shenoy, D. Fusco, S. M. Janicki, D. L. Spector and R. H. Singer, *Science*, 2004, **304**, 1797-1800.

4 (a) J. S. Paige, T. Nguyen-Duc, W. Song and S. R. Jaffrey, *Science*, 2012, **335**, 1194; (b) W. Song, G. S. Filonov, H. Kim, M. Hirsch, X. Li, J. D. Moon and S. R. Jaffrey, *Nat. Chem. Biol.*, 2017, **13**, 1187-1194.

5 (a) S. Tyagi and F. R. Kramer, *Nat. Biotechnol.*, 1996, **14**, 303-308; (b) S. Tyagi, D. P. Bratu and F. R. Kramer, *Nat. Biotechnol.*, 1998, **16**, 49-53.

6 (a) T. Ozawa, Y. Natori, M. Sato and Y. Umezawa, *Nat. Methods*, 2007, **4**, 413-419; (b) H. Yoshimura, A. Inaguma, T. Yamada and T. Ozawa, *ACS Chem. Biol.*, 2012, **7**, 999-1005.

7 (a) A. Murata, S. Sato, Y. Kawazoe and M. Uesugi, *Chem. Commun.*, 2011, **47**, 4712-4714; (b) S. Sato, M. Watanabe, Y. Katsuda, A. Murata, D. O. Wang and M. Uesugi, *Angew. Chem. Int. Ed.*, 2015, **54**, 1855-1858; (c) S. Sato, K. Yatsuzuka, Y. Katsuda and M. Uesugi, *Methods Mol. Biol.*, 2018, **1649**, 305-318; (d) A. Arora, M. Sunbul and A. Jaschke, *Nucleic Acids Res.*, 2015, **43**, e144.

8 S. A. Marras, *Methods Mol. Biol.*, 2006, **335**, 3-16.

9 S. Hirayama, Y. Hori, Z. Benedek, T. Suzuki and K. Kikuchi, *Nat. Chem. Biol.*, 2016, **12**, 853-859.

10 D. Kosman, C. M. Mizutani, D. Lemons, W. G. Cox, W. McGinnis and E. Bier, *Science*, 2004, **305**, 846.

11 S. Jain, J. R. Wheeler, R. W. Walters, A. Agrawal, A. Barsic and R. Parker, *Cell*, 2016, **164**, 487-498.

A multicolor RNA imaging technology permits direct observation of stress granule formation in living cells.

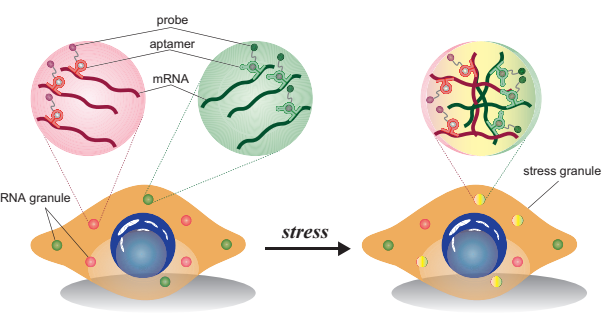
probe
aptamer
mRNA
RNA granule
stress
stress granule